Solar Reflector Design

Report Contributors: Afonso Bandeira[1] , Christopher G. Bell [2], Jean P.F. Charpin[3,4], Romina Gaburro[3], Sofiane Soussi[3] and R. Eddie Wilson[5]

Study Group Contributors: Giles Richardson[6] and Galin Ganchev[3]

Industry Representative: Sean Hoolan[7]

[1]Universidade de Coimbra, Portugal
[2]Department of Bioengineering, Imperial College London, United Kingdom
[3]MACSI, department of Mathematics and Statistics, University of Limerick, Limerick, Ireland
[4]Report coordinator, jean.charpin@ul.ie
[5]Department of Engineering Mathematics, University of Bristol, United Kingdom
[6]School of Mathematics, University of Southampton, United Kingdom
[7]Erin Energy Ltd, Applied Research into Solar Technologies, MIRC Building, Athlone Institute of Technology, Dublin Road, Athlone, Co Westmeath, Ireland

Abstract

The design of solar panels is investigated. Different aspects of this problem are presented. A formula averaging the solar energy received on a given location is derived first. The energy received by the collecting solar panel is then calculated using a specially designed algorithm. The geometry of the device collecting the energy may then be optimised using different algorithms. The results show that for a given depth, devices of smaller width are more energy efficient than those of wider dimensions. This leads to a more economically efficient design.

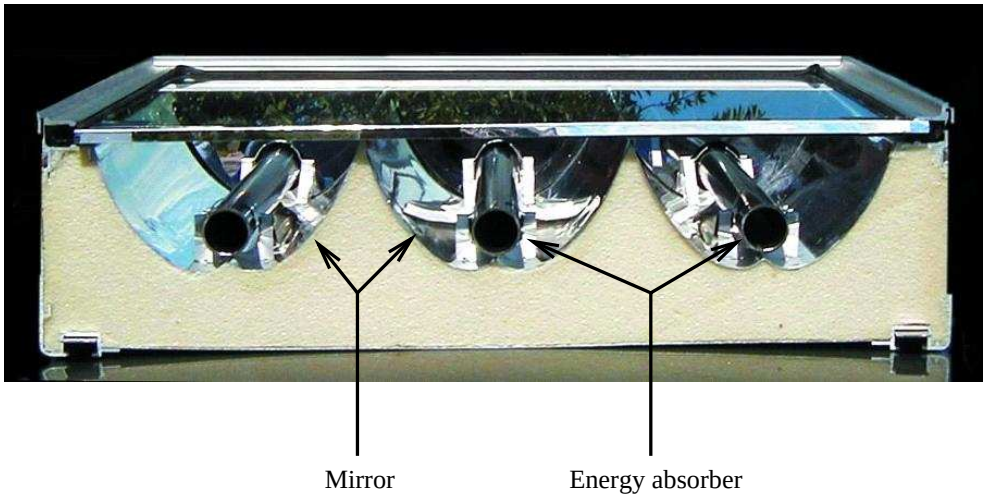

Figure 1: Typical configuration

1 Introduction

In recent years, considerable research was carried out on renewable sources of energy. Designing cheap and efficient devices has become a priority for the industry. Erin Energy, based in Athlone, Westmeath, Ireland, is focusing on solar energy. A typical example of design they study may be seen on Figure 1. This device should be placed on the roof. The solar energy is collected by the energy absorber, transported and then stored in a chemically based energy tank. Ideally, the roof should be completely covered with energy collectors but they are quite expensive. To reduce the amount of collectors necessary, the roof is covered with mirrors. The solar energy may then be collected either directly or after one or more reflections on the mirrors. The shapes of the mirrors and collectors are key to the efficiency of the system. Erin Energy currently investigates a cylindrical collector coupled with parabolic or involute shaped mirrors. They would like to evaluate the efficiency of their current design and if possible, find more optimised shapes. This problem was submitted to the the 70th European Study Group in Industry held in Limerick in June-July 2009. This report reflects the work of the group.

Different directions were investigated to tackle this problem. First of all, the incoming solar energy was considered. This parameter varies with the position of the device, its inclination, the time of the day and the time of the year. These different aspects were considered and are detailed in Section 2. The reflections of rays and energy over the mirror was then considered. An exact and fast ray tracing algorithm was developed in MATLAB and is presented in Section 3. Several methods were then considered to optimise the shape of the mirrors. An approach based on inverse methods is introduced in Section 4. An alternative was developed to maximise the direct and first reflections. This aspect is detailed in Section 5. Finally a more general optimisation based on a pattern search method was used and the results may be found in Section 6.

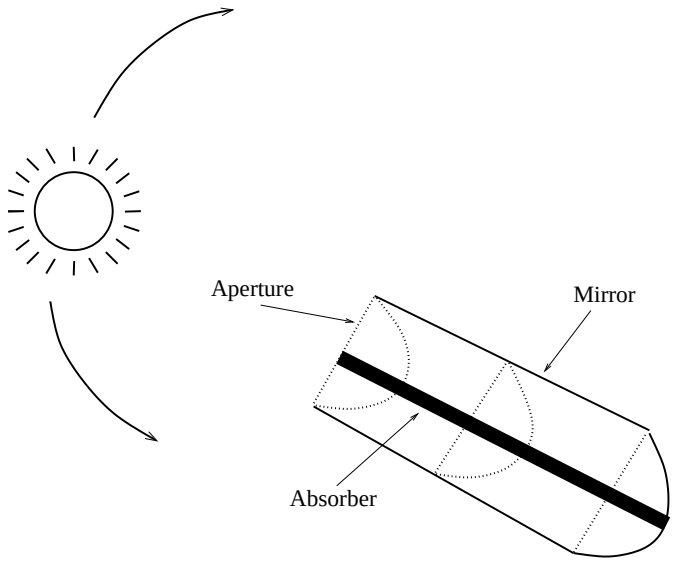

Figure 2: Sketch of a trough-like solar concentrator.

2 Model for annual energy collection

To calculate the annual energy collected by a stationary trough-like solar concentrator such as that pictured in Figure 2 requires two steps. Firstly we must find the energy incident on the aperture as a function of the position of the sun, and then we must calculate how much of this energy is transmitted to the absorber via reflections from the mirror. In all of this work, we only consider direct beam radiation and ignore the effects of diffuse radiation. For a concentrator situated at latitude angle ϕ, a simple model for the total annual energy collected may be written as

$$E_{\text{annual}} = \mathcal{A} \int_{-\delta_{\max}}^{\delta_{\max}} \int_{0}^{\omega_{\lim}(\delta,\,\phi)} F(\delta,\,\omega,\,\phi)\, \mathcal{T}(\delta,\,\omega,\,\phi)\, d\omega\, d\delta. \tag{2.1}$$

The *energy function* $F(\delta,\,\omega,\,\phi)$ models the energy striking a unit area of the aperture, and multiplying by the area $\mathcal{A}$ of the aperture gives the total energy entering the aperture. The *transmission function* $\mathcal{T}(\delta,\,\omega,\,\phi)$ $(0 \leq \mathcal{T} \leq 1)$ models the fraction of the energy entering the aperture which hits the absorber. Integrating over δ and ω sums the total energy collected over the year.

The parameter δ is the declination angle [1, 2], which varies between $\pm\delta_{\max} = \pm 0.40928$ radians and determines the height of the Sun above the equatorial plane throughout the year. The variation of δ as a function of day number N, with $N = 1$ being the 1st January, is depicted in Figure 3.

The rotation of the Earth is measured by the hour angle, ω [1, 2], and the range of integration $[0, \omega_{\lim}(\delta,\,\phi)]$ is determined by the hours of daylight available to the concentrator. This

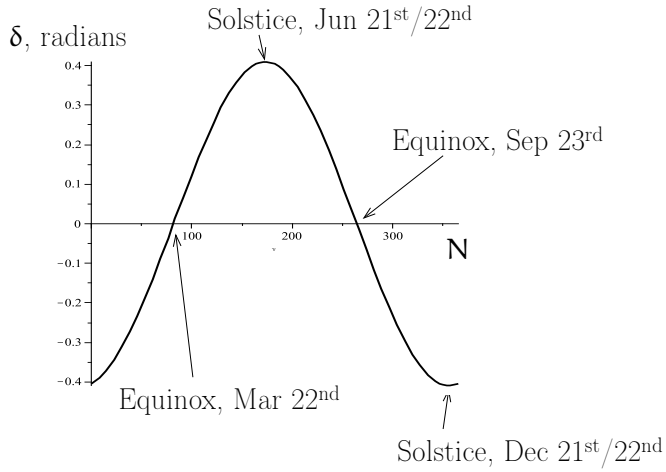

Figure 3: Graph of how the declination angle δ varies as a function of the day number N.

depends both on the height of the Sun in the sky (which depends on δ and ϕ) and on the orientation and angle of tilt of the concentrator.

The function $F(\delta, \omega, \phi)$ models the intensity of the light striking the aperture of the concentrator as a function of δ and ω, corresponding to particular times of day and season. A general formula for $F(\delta, \omega, \phi)$ may be written as [3]

$$\begin{aligned} F(\delta, \omega, \phi) = 4 \times I_{sc} \times \frac{43200 \times 365.25}{2\pi^2} \times \\ \left[1 + \frac{0.034}{\sin(\delta_{max})} \cos\left(\frac{2\pi}{365.25} \times 173\right) \sin\delta\right] \times \\ \left(a_0 + a_1 \exp\left(-\frac{k}{\cos\delta \cos\omega \cos\phi + \sin\delta \sin\phi}\right)\right) \times \\ \mathbf{s}(\delta, \omega, \phi) \cdot \mathbf{n} \times \\ \frac{\cos\delta}{\sqrt{\sin^2(\delta_{max}) - \sin^2\delta}}. \end{aligned} \tag{2.2}$$

In this formula, the first line quantifies the amount of radiation striking the outer edge of the earth's atmosphere. The parameter $I_{sc} = 1367$ W m^{-2} is the solar constant [2] and the multiplicative factor results from changing the integration parameters from time to angle. The second line adjusts for the ellipticity of the earth's orbit around the Sun [2]. The third line models the reduction in the intensity of the light striking the earth's surface depending on how far it has travelled through the atmosphere. We use the Hottel model [4], and we take the 23km Visibility Haze parameters at zero altitude:

$$a_0 = 0.1281, \quad a_1 = 0.7569, \quad k = 0.3872. \tag{2.3}$$

The fourth line measures the 'cosine effect' and modifies the energy striking the aperture according to the angle of incidence. Here $\mathbf{s}(\delta, \omega, \phi)$ is a vector pointing in the direction of the

Sun and $\mathbf{n}$ is the normal vector to the aperture of the collector. Finally the last line comes from the Jacobian due to the change in variables of integration from time to angle.

For trough-like concentrators, the problem of calculating the fraction of energy, $\mathcal{T}(\delta, \omega, \phi)$, transmitted from the aperture to the absorber is essentially two-dimensional. Away from the ends of the trough, the component of the energy flux along the longitudinal axis may be ignored and the energy collected is simply a function of the angle of incidence in the plane orthogonal to the longitudinal axis of the concentrator. We call this angle $\xi(\delta, \omega, \phi)$ $(-\pi/2 \leq \xi \leq \pi/2)$, and measure it relative to the normal to the aperture of the concentrator as shown in Figure 4. This angle of incidence is a function of the position of the Sun (through δ, ω and ϕ), and also depends on the orientation and tilt of the concentrator. For a particular shape of mirror and position of absorber, it is easy to calculate $\mathcal{T}(\xi)$ for any angle of incidence ξ by using ray tracing, and if we know how ξ depends on δ, ω and ϕ, we may calculate the energy integral.

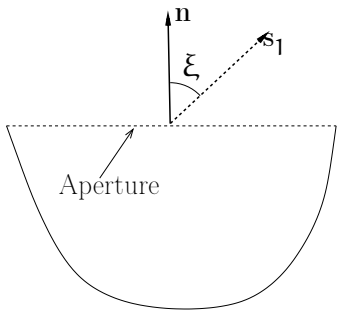

Figure 4: Sketch showing the angle of incidence ξ in the plane orthogonal to the longitudinal axis of the concentrator. The vector $\mathbf{s_1}$ is the projection of the vector $\mathbf{s}$ pointing in the direction of the Sun into this plane and $\mathbf{n}$ is the normal to the aperture.

To assess the performance of a concentrator, there are therefore four functions to determine before the annual energy may be calculated

- $\omega_{\lim}(\delta, \phi)$ - the hours of daylight available to the concentrator;
- $\mathbf{s}(\delta, \omega, \phi) \cdot \mathbf{n}$ - the 'cosine effect ' due to the angle of incidence of the energy onto the aperture;
- $\xi(\delta, \omega, \phi)$ - the angle of incidence in the plane orthogonal to the longitudinal axis of the concentrator;
- $\mathcal{T}(\xi)$ - the fraction of incident energy transmitted to the absorber as a function of the angle of incidence ξ.

The first three functions depend on the orientation and tilt of the concentrator, while the last depends on the shape of the mirror and the position of the absorber.

In reference [3], we have considered the above problem for a horizontal east-west aligned concentrator tilted at an angle θ_n from the vertical. If we restrict the location of the concentrator to be between the Antarctic and Arctic circles so that

$$\delta_{\max} - \frac{\pi}{2} \leq \phi \leq \frac{\pi}{2} - \delta_{\max}, \tag{2.4}$$

and we restrict the angle of tilt θ_n so that

$$-\phi - \left(\frac{\pi}{2} - \delta_{\max}\right) \leq \theta_n \leq -\phi + \left(\frac{\pi}{2} - \delta_{\max}\right), \tag{2.5}$$

then it is possible to show that the hours of daylight are specified by the upper limit

$$\omega_{\lim}(\delta,\, \phi,\, \theta_n) = \min\left[\arccos\big(-\tan\delta\tan(\phi+\theta_n)\big),\ \arccos\big(-\tan\delta\tan\phi\big)\right]. \tag{2.6}$$

The restriction on the angle of tilt θ_n is reasonable, since as a general rule of thumb using the polar mount (or $\theta_n = -\phi$) for an east-west concentrator is close to maximizing the annual energy incident on the aperture [1]. The 'cosine effect' is specified by the relationship

$$\mathbf{s}(\delta,\, \omega,\, \phi)\cdot\mathbf{n} = \cos\delta\cos\omega\cos(\phi+\theta_n) + \sin\delta\sin(\phi+\theta_n), \tag{2.7}$$

and finally the angle ξ may be calculated through the relationship [5]

$$\xi(\delta,\, \omega,\, \phi) = -\theta_n - \phi + \tan^{-1}\left(\frac{\tan\delta}{\cos\omega}\right). \tag{2.8}$$

For further information on determining the above functions for different orientations and tilts, see references [1, 2].

As a final comment, in reference [3] for a horizontal tilted east-west concentrator, we show how to change integration variables from $(\delta,\, \omega)$ to $(\delta,\, \xi)$ so that the energy integral may be written in the form

$$E_{\text{annual}} = \mathcal{A}\int\int F(\delta,\, \xi,\, \phi)\,\mathcal{T}(\xi)\,d\delta\,d\xi. \tag{2.9}$$

It is then easy to substitute in for the transmission function as a direct function of ξ. In the next section we show how to develop a ray tracing algorithm to calculate $\mathcal{T}(\xi)$.

3 Ray-tracing package

3.1 Motivation and scope

Later in this report we shall propose several different methods for generating reflector shapes. These are based on either heuristic techniques, or on the formal optimisation of energy return in some highly simplified setting — for example, we may neglect all secondary reflections or

consider only a reduced model for the trajectory of the sun through the sky and its effective intensity as a function of inclination.

Whatever approach is used to generate reflector shapes, there is a need to definitively evaluate the return in a realistic setting which captures the full details of energy collection throughout the year and which may also cope with extra effects such as diffuse radiation (which is thought to be important in an Irish setting). This definitive evaluation can only be carried out numerically, and the computational framework that we implemented is based on the classical approach of ray-tracing.

There are in fact many ray-tracing packages already in the public domain which are equal to our task, but none that we found are specialised to the particular geometry etc. of solar reflector design, yet flexible enough for our computational experiments. In summary, it seemed best to implement our own ray-tracing package during the Study Group itself, using the high-level computational language Matlab.

Our code took only about one man-day to complete and forms the basis of a very pleasing tool with which reflector design can be investigated. The user has access to all the powerful programming and visualisation features of the Matlab environment, yet at the same time, the computational kernel is sufficiently fast that meaningful calculations can be carried out almost instantaneously on even modest laptop hardware.

Later in the report, we describe how we drove the ray-tracing code in the inner loop of a black box optimisation algorithm, thus enabling formal optimisation of the reflector profile even for realistic models of incident radiation. This is an extremely demanding problem from the computational point of view, yet the optimisation proved tractable provided the search was restricted to relatively simple reflector designs. Of course, it will be possible to accelerate run times significantly, and thus attempt more sophisticated optimisation (over wider search spaces and resolving more detail of the reflector profile), by either translating the computational kernel into a low-level language such as C or Fortran, or porting the code to specialised parallel hardware such as GPU machines. These tasks remain for future work, as does the development of a polished graphical front-end.

Since we consider only reflectors with a fixed cross-section, we may simplify matters by only tracing rays constrained to the plane of the cross-section. In reality, at most times of day real-world rays will have an out-of-plane component, but this may be compensated for by a reduction in the intensity factor. Here we assume that the reflector is much longer than it is wide so that end-effects may be neglected.

3.2 Interface to the computational routine

In summary, we need only perform ray-tracing in two dimensions, where the reflector is modelled by a curve and the absorber element by a circle. As a final simplification, we disretise the reflector by approximating it by a set of straight line segments, since the intersection of

straight lines (rays) with straight lines (reflector segments) is a particularly simple computational problem. The accuracy of results may then be refined by increasing the number of line segments used in the discretisation: order several hundred to a thousand segments is tractable with standard hardware.

The inputs to our routine are thus:

- The radius $R > 0$ of a single circular absorber element $\|\mathbf{r}\| = R$, with centre placed at the origin, so that all other coordinates are expressed relative to it.
- A collection of $i = 1, 2, \ldots, m$ straight line reflector segments, described in terms of the position vectors $\mathbf{a}^{(i)}$ and $\mathbf{b}^{(i)}$ of their end-points.
  - In practice, we will often have $\mathbf{a}^{(2)} = \mathbf{b}^{(1)}$, $\mathbf{a}^{(3)} = \mathbf{b}^{(2)}, \ldots$, so that the segments join together to give a contiguous curve, but these conditions are not required by the code, so reflectors consisting of several disconnected components may also be tested.
- A collection of $j = 1, 2, \ldots, n$ rays, prescribed in terms of their starting points $\mathbf{r}_0^{(j)}$ and unit directions $\hat{\mathbf{t}}^{(j)}$. In practice, this ensemble may consist of:
  1. Sets of parallel rays with different starting points arranged uniformly along a straight line segment above the reflector so that the complete set of rays is incident across the width of the reflector's aperture. This set-up tests the energy collection for a single incident angle.
  2. Ensembles of ensembles of type 1., so many incident angles can be tested simultaneously.
  3. Ensembles of non-parallel rays to test diffuse radiation.
- The maximum number p of reflections that should be computed for each individual ray.

The output of the routine is:

- The eventual 'fate' of each ray. The possibilities are:
  1. Ray hit absorber element after k reflections on the solar reflector, $0 \leq k \leq p$.
  2. Ray 'escapes to infinity' after k reflections, $0 \leq k \leq p$, so that it could not be incident upon the absorber even if the parameter p were increased.
  3. Ray is 'in-play' after p reflections, in that it has yet to hit the absorber or escape to infinity. The fate of the ray can only be decided by experimenting with larger values for p. In practice we fix p at a sufficiently large value (e.g. 5 or 6) so that only a very small proportion of rays fall in this category.

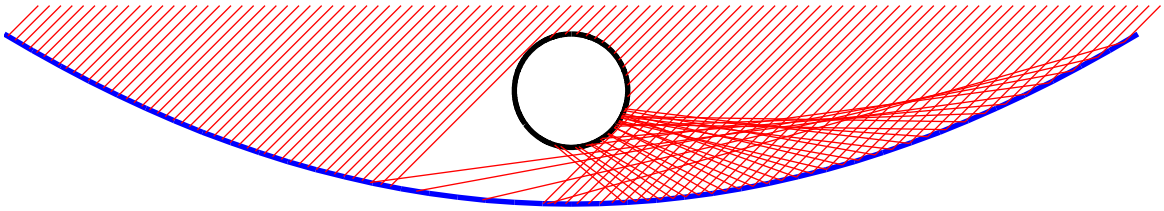

Figure 5: Simple output from the ray-tracing routine. A small ensemble of parallel rays are shown incident upon a parabolic reflector discretised into 200 straight line segments. Reflections to infinity are not shown. In this configuration no ray is reflected more than twice, but larger numbers of reflections may be tracked. Here the circular absorber intercepts the caustic of the reflector and so is particularly efficient at capturing the incident radiation.

In verbose mode, the user also has access to diagnostic information giving the full itinerary of each ray in terms of the indices of the reflector segments that it hit, and the points at which it was reflected. The latter data may be used to drive a plotting routine: example output is shown in Fig. 5.

An energy collection calculation must then weight the output of the routine according to the nature of each ray (position of the sun etc., incorporating the factors from Section 2) which hits the absorber and by α^k, where k is the number of reflections it has suffered in the mean time and α is the reflectivity. Rays which are of types 2. or 3. are given zero weight. The total energy return is then just the scalar obtained by summing over all rays.

3.3 Computational method

We now give a brief description of how the computational kernel works. In essence, it operates serially over the reflection number $k = 1, 2, \ldots, p$ but for a given k the code is vectorised over all rays and reflector segments. This vectorisation means all the hard number crunching is performed internally in Matlab commands rather than by interpreted loops — and this is the key factor in the code's speed. This structure also means that the code should port to parallel architectures rather simply.

- For reflection numbers from $k = 0$ to $k = p$ in sequence:
  - For *all* combinations of admissible reflector segments $i = 1, 2, \ldots, m$ and rays $j = 1, 2, \ldots, n$, find potential intersections by solving the 2×2 system

$$\lambda^{(i,j)}\mathbf{a}^{(i)} + (1 - \lambda^{(i,j)})\mathbf{b}^{(i)} = \mathbf{r}_0^{(j)} + s^{(i,j)}\hat{\mathbf{t}}^{(j)} \tag{3.1}$$

    for $\lambda^{(i,j)}$ and $s^{(i,j)}$ simultaneously.

– Mark intersections as *allowable* if $0 \leq \lambda^{(i,j)} < 1$ and $s^{(i,j)} > 0$, since each reflector component is a finite line segment and each ray is in fact a half-line starting at $\mathbf{r}_0^{(j)}$. Here we consider half-open reflector segments to avoid double counting problems where the segments are knotted together at their end-points.

– For each ray j, compute

$$s_*^{(j)} = \min_{\text{allowed } i} s^{(i,j)}, \tag{3.2}$$

and let $i_*^{(j)}$ denote the arg min. This means that ray j will next hit reflector segment $i_*^{(j)}$ after distance $s_*^{(j)}$, unless it hits the absorber first.

– For each ray j, also consider intersections with the absorber by solving the quadratic

$$\|\mathbf{r}_0^{(j)} + \tilde{s}^{(j)}\hat{\mathbf{t}}^{(j)}\|^2 = R^2 \tag{3.3}$$

for $\tilde{s}^{(j)}$. Here we are of course interested only in real solutions with $\tilde{s}^{(j)} > 0$. In the case of two such solutions, we take the least (corresponding to the first intersection). In fact, the case of real solutions with opposite signs will generally not occur in practice since this corresponds to rays that start inside the absorber element!

– Some control logic is now applied to each ray (but this is also vectorisable). If there is an allowable $\tilde{s}^{(j)} > 0$ then either

- $\tilde{s}^{(j)} < s_*^{(j)}$, in which case ray j next hits the absorber element, and the number of reflections $k^{(j)}$ suffered so far is recorded. No further computation is required for this ray and it should be removed from the computation: however, the vectorisation works most efficiently if it is left in the computation with a dummy flag indicating that the control logic steps should not be applied to it in future.
- $\tilde{s}^{(j)} > s_*^{(j)}$, in which case ray j next hits reflector segment $i_*^{(j)}$. In this case, the new starting point $\mathbf{r}_0^{(j)}$ of the ray is re-set to

$$\mathbf{r}_0^{(j)} + s_*^{(j)}\hat{\mathbf{t}}^{(j)}, \tag{3.4}$$

and its new unit direction $\hat{\mathbf{t}}^{(j)}$ is then set to

$$\hat{\mathbf{t}}^{(j)} - 2(\hat{\mathbf{t}}^{(j)} \cdot \hat{\mathbf{n}}^{(i_*^{(j)})})\hat{\mathbf{n}}^{(i_*^{(j)})}, \tag{3.5}$$

corresponding to reflection, where $\hat{\mathbf{n}}^{(i)}$ is the unit normal of reflector segment i, which is computed one-shot at the start of the routine from $\mathbf{a}^{(i)}$ and $\mathbf{b}^{(i)}$. Finally, reflector segment $i_*^{(j)}$ is marked as an inadmissible hit for ray j at the next iteration and remains so for further iterations until ray j hits some other reflector segment. This fix is to avoid 'double hit' problems due to rounding error, where $\mathbf{r}_0^{(j)}$ is placed marginally on one (the wrong) side of the reflector segment, so that it almost instantaneously next hits the same segment. The consequent spurious effect is that some rays appear to pass straight through reflector segments without deviation — hence the admissibility flag which fixes this problem is of key importance.

- There are also a number of 'empty' cases which must be covered but which we shall not enumerate in detail. For example, in the case where there is no allowable hit with the absorber, the first hit with the reflector should still be processed. If there are no allowable / admissible hits with the reflector, the first hit with the absorber should still be processed. If there are no allowable / admissible hits with either the absorber or the reflector, then the ray in question has escaped to infinity and is marked as such.

- Loop over reflection number k.

Note. Here the sense $\hat{\mathbf{n}}^{(i)}$ of the reflector segment is not considered, so in effect each reflector segment is a two-sided mirror. The generalisation to one-sided mirrors with a matt reverse side is easily achievable, but requires extra control logic which we have yet to implement.

Using the models and algorithms developed in this section and Section 2, work will now focus on the shape of the mirror. Three approaches will be presented: the inverse problem will be detailed first, followed by two optimisation methods.

3.4 Computational cost

The run-time of our routine scales like $O(mnp)$, i.e., it is linearly proportional to each of the number of reflector segments, rays, and reflections considered. In addition, the memory constraints scale like $O(mn)$ due to the Matlab vectorisation techniques used, but a C or Fortran code could be optimised to scale like $O(m)$ in this respect. In practice, we have found that the routine takes just a couple of seconds on a laptop when $mnp \sim 10^6$.

Clearly the bottleneck in our approach is the consideration at each iteration of all possible intersections between all rays and all reflector segments. It may be possible to speed-up matters by reducing the search space: for example, we may segment the plane into rectangular sub-regions and index reflector segments by which rectangle they belong to. The itinerary of each ray through the sub-regions may then be used to seek intersections with reduced lists of reflector segments. It seems plausible that this approach may give a $O(\sqrt{m})$ or $O(\log m)$ speed-up, but with a significant coding burden which we have yet to undertake. Moreover, this refinement would break the Matlab vectorisation so would only be worthwhile for a low-level language implementation. These features remain for future work.

4 Inverse problem

In this section we consider the 2-dimensional case in which the absorber is a point source located at the origin of the xy axes in $\mathbb{R}^2$ and the position of the Sun is given by an angle θ, for $0 \leq \theta \leq \pi$ (anticlockwise). Although in a more realistic situation the absorber would be

described by a circle centred at the origin $(0,0)$, the case of a point source collector seems the most appropriate simplified situation to be investigated. The modification in the mathematical model required for the more realistic circle case will be considered later on.

Let us recall that the goal is to find the best shape of a mirror placed nearby the source in order to maximise the number of reflections of rays coming from the Sun into the absorber. In the inverse problem we consider the following approach. The case in which radiation is emitted from the absorber is considered. The electromagnetic radiation is emitted in all directions and reflected from the nearby mirror. The goal is to model the reflected rays in term of the incident field coming from the absorber and the shape of the mirror. The inversion consists then in two steps: i) image the mirror in terms of the reflected rays, ii) find the best shape for the mirror by prescribing the reflected rays with some conditions that maximise the number of reflections from the mirror to the general receiver's location (sun's location). Let us specify our problem.

4.1 The mathematical model

The incident field

Let us denote by $X = (x, y)$ any point in $\mathbb{R}^2$. We consider the simple scalar wave equation to model the wave propagation. We make the following assumption.

Assumption 4.1. *We assume that the mirror is well separated from the region where the sensors are located and that in the intervening region* $c(x) = c_0$*, where* c_0 *is the (assumed constant) speed of light in air.*

The above assumption is reasonable since the sensors location coincide with the sun's location.

The incident field due to a delta source located at $(0,0)$ at time $t = 0$ satisfies

$$\left(\nabla^2 - \frac{1}{c_0^2}\partial_t\right) u^{in}(t, X) = -\delta(X)\delta(t), \tag{4.1}$$

therefore, at the point X, at the time t', it is simply the Green's function G_0 associated to the wave operator appearing on the left hand side of (4.1)

$$u^{in}(t', X) = G_0(t', X) = \frac{\delta\left(t' - \frac{|X|}{c_0}\right)}{4\pi|X|}.$$

The reflected field

We start by giving two definitions.

DEFINITION 4.1. *We denote by* $\mathcal{M} = \{(x, f(x)) \mid x \in \mathbb{R}\}$ *the graph of some function* $f : \mathbb{R} \to \mathbb{R}$ *which represents the shape of the mirror.*

DEFINITION 4.2. *We denote by* $R(\theta) = (R_x(\theta), R_y(\theta))$ *the location of the receiver (the sun) at the angle* θ *from the ground.*

If c_0 is the speed of light in the air introduced above, we assume that the perturbation in wave speed c takes the form

$$V(X) := \frac{1}{c_0^2} - \frac{1}{c^2(X)} = \tilde{V}(x)\delta(y - f(x)), \tag{4.2}$$

where V is the *reflectivity function* and it represents the change in speed of the ray when it hits the mirror at the point $X = (x, f(x))$. We write the total field u as the sum

$$u = u^{in} + u^{rf},$$

where u^{rf} represents field reflected from the mirror. The total field u satisfies

$$\left(\nabla^2 - \frac{1}{c^2(X)}\partial_t\right) u(t, X) = -\delta(X)\delta(t) \tag{4.3}$$

By combining (4.1) and (4.3) we obtain

$$\left(\nabla^2 - \frac{1}{c^2(x)}\partial_t\right) u^{rf}(t, X) = -V(X)\partial_t^2 u. \tag{4.4}$$

Linearised problem

We rewrite (4.4) in integral form and make use of the *Born Approximation* (single scattering approximation) to replace the total field u on the right hand side of (4.4) with the incident field u^{in}

$$u^{rf}(t, \theta) = \mathbf{F}V(t, \theta) = \int \frac{e^{-i\omega(t-(|R(\theta)-X|+|X|)/c_0)}}{(4\pi)^2|R(\theta) - X||X|}\, \omega^2\, V(X) d\omega\, dX. \tag{4.5}$$

This approximation linearises the problem because the product of unknowns Vu on the right hand side of (4.4) is replaced by the product of the unknown V with the known incident field u^{in}. If we denote by

$$A(X,\theta,t,\omega) := \frac{\omega^2}{(4\pi)^2|R(\theta)-X||X|},$$

we obtain

$$U^{rf}(t,\theta) = \mathbf{F}V(t,\theta) = \int e^{-i\omega(t-(|R(\theta)-X|+|X|)/c_0)}\, A(X,\theta,t,\omega)\, V(X) d\omega\, dX, \tag{4.6}$$

where ω denotes the angular frequency and $\mathbf{F}$ is the *forward map* which maps the reflectivity function into the reflected ray collected at different location θ and different *travel time* t.

Remark 4.2. *Notice that the support of* V, $\mathrm{supp}(V)$ *satisfies*

$$\mathrm{supp}(V(x,y)) \subset \{(x,y) \in \mathbb{R}^2 \,|\, y = f(x)\},$$

i.e. finding V *is equivalent of finding the curve* $y = f(x)$.

4.2 Inversion

Microlocal analysis

$\mathbf{F}$ is a Fourier Integral Operator (FIO) given by the oscillatory integral (4.6) with phase function

$$\phi(\theta,t,x,\omega) = -\omega\Big[t - (|R\big(\theta\big) - X| + |X|)/c_0\Big] \tag{4.7}$$

FIOs are well-studied operators and the imaging scheme planned to be used here will be based on FIO theory, which is part of microlocal analysis [6, 7, 8]). Singularity in the scene are mapped into singularity in the data by the so-called *canonical relation* of F, Λ_F

$$\Lambda_F = \Big\{\Big((\theta,t;\sigma,\tau),(X,\xi)\Big) \,|\, \begin{array}{l} D_\omega(\theta,t,X,\omega) = 0 \\ \sigma = D_\theta\phi \\ \tau = D_t\phi \\ \xi = D_X\phi\Big\}. \end{array} \tag{4.8}$$

For F given by (4.6) we have

$$\Lambda_F = \left\{ \Big((\theta, t; \sigma, \tau), (X, \xi) \Big) \mid \quad \begin{aligned} t &= \frac{1}{c_0}(|R(\theta) - X| + |X|) \\ \tau &= -\omega \\ \sigma &= \frac{\tau}{c_0} \widehat{R(\theta) - X} \cdot \dot{R}(\theta) \\ \xi &= \frac{\tau}{c_0}(\widehat{R(\theta) - X} - \widehat{X}) \end{aligned} \right\}. \tag{4.9}$$

The first condition in (4.9) is a travel time condition

$$\begin{aligned} t^2 &= |R(\theta) - X|^2 + |X|^2 \\ &= (h\cos(\theta) - x)^2 + (h\sin(\theta) - f(x))^2 + x^2 + f^2(x) \end{aligned}$$

and it represents the set of points of intersection between the ellipse with foci the sun's location $R(\theta)$ and the absorber's location $(0, 0)$ with the curve $y = f(x)$ we want to reconstruct. The second condition of (4.9) (σ-condition)

$$\sigma = \frac{\tau}{c_0} \widehat{R(\theta) - X} \cdot \dot{R}(\theta)$$

gives us the correct point we want to image X and its reflection across the velocity field $\dot{R}(\theta)$: this is not relevant since the mirror is obviously located below the $R(\theta)$, therefore this condition will not introduce artefacts in the image.

Formation of the image

We use a *filtered back projection* operator to form the image, i.e. we apply a filtered adjoint of the forward operator to the data: this operator has the same phase as the adjoint of F, with the filter to be chosen later. The image of X is given by

$$I(X) := \int e^{i\omega(t - (|R(\theta) - X| + |X|)/c_0)} \, B(X, \theta, t, \omega) U^{rf}(\theta, t) d\omega d\theta dt. \tag{4.10}$$

If we combine (4.10) together with (4.6) we obtain

$$I(X) = \int K(X, X') V(X') dX', \tag{4.11}$$

where

$$K(X,X') = \int e^{-i\omega((|R(\theta)-X|+|R(\theta)-X'|)/c_0)}\, A(Z,\theta,|X'-R(\theta)|,\omega)B(X,\theta,|X-R(\theta)|,\omega)d\omega d\theta.$$

The kernel $K(X,X')$ is the imaging *point spread function* and it arises because it is the image that would result from a delta function located at the point X'. If we perform a large-ω stationary phase analysis of K, it turns out that the main contribution to K does indeed arise from the point $X = X'$ as predicted in subsection 2.1. This is quite a well known machinery that have been used in the community working on this kind of problem [9, 10, 11, 12, 13, 14]).

By making use of the above method we can therefore obtain an image of the mirror $y = f(x)$ in terms of the reflected rays. The work that needs to be done in the future is the understanding of how optimising the shape of the mirror would influence the general reflected ray $U^{rf}(\theta,t)$. We believe that an approach to investigate should be the one of maximising the number of possible travel times of the total field arriving at the same location θ.

5 One reflection construction

In this section the shape of the mirrors is determined to maximise the amount of energy collected by the energy collector for a given width of the aperture. The optimisation is carried out by considering direct illumination and first reflections through the entire day. The position of the collector is determined first, then the amount of reflected energy is calculated. Finally, a simple optimisation algorithm is used to determine the shape of the mirror. The geometry is determined using the following assumptions:

- The length of the aperture is fixed,
- The collector is a cylinder of given radius,
- The device is optimised for a flat position,
- The position of the collector is maximised for a Sun angle of incidence $\theta_0 < \theta < \pi - \theta_0$, where θ_0 is a small given angle.

5.1 Position of the collector

To maximise direct energy hits, the collector should be positioned as high as possible above the roof surface. However, if placed too high, a collector will create shadow on the next element and limit its efficiency. A typical configuration is shown on Figure 6.

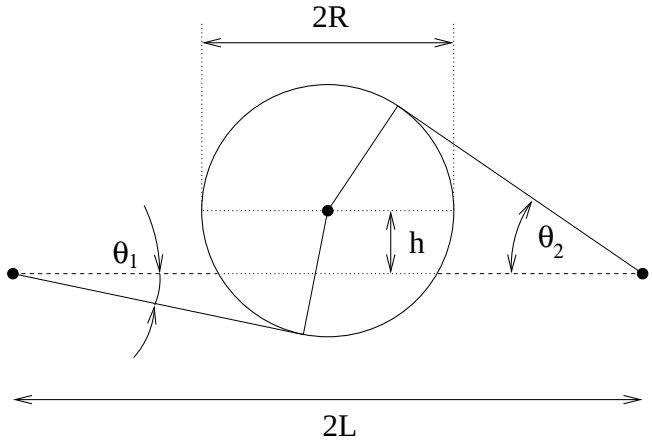

Figure 6: Position of the collector.

A simple geometry calculation shows that the height H of the centre of the collector may be expressed as:

$$h_1 = \frac{L \sin\theta_1 + R}{\cos\theta_1} , \qquad h_2 = \frac{L \sin\theta_2 - R}{\cos\theta_2}$$

where L denotes half the length of the aperture and R is the radius of the collector cylinder. If the collector is positioned to maximise angles $\theta_0 < \theta < \pi - \theta_0$, as is obvious from the figure, the shadow of the cylinder on the next element, described by the angle θ_2, will be the limiting factor and the height of the cylinder should be:

$$h = \frac{L \sin\theta_0 - R}{\cos\theta_0} . \tag{5.1}$$

5.2 First reflection

The shape of the mirror will now be defined. To start with, the energy reflected by one element of mirror will be calculated and then a simple optimisation algorithm will be developed.

Energy reflected

We consider a cylindrical absorber of radius R placed above a reflector having some arbitrary shape extending between edges $A_\pm$ with the coordinates $(\pm d, h)$. The problem is supposed to be invariant by translation along the absorber axis which allows us to consider the problem in a 2D geometry. We use the Cartesian coordinate system (O, x, y) as shown on Figure 7.

The Sun position is given by the angle θ between the horizontal and the line going through the Earth and the Sun centres. The Sun is assumed to have a uniform circular motion so that there is an equivalence between the variable θ and the time. For a general point M taken on

the reflector surface, we denote by (x_M, y_M) its coordinates in our coordinate system. , τ the tangent vector oriented from A_- to A_+, and ν the normal vector that is τ rotated by $\pi/2$. Finally we call α the algebraic angle between the x-axis and the vector τ.

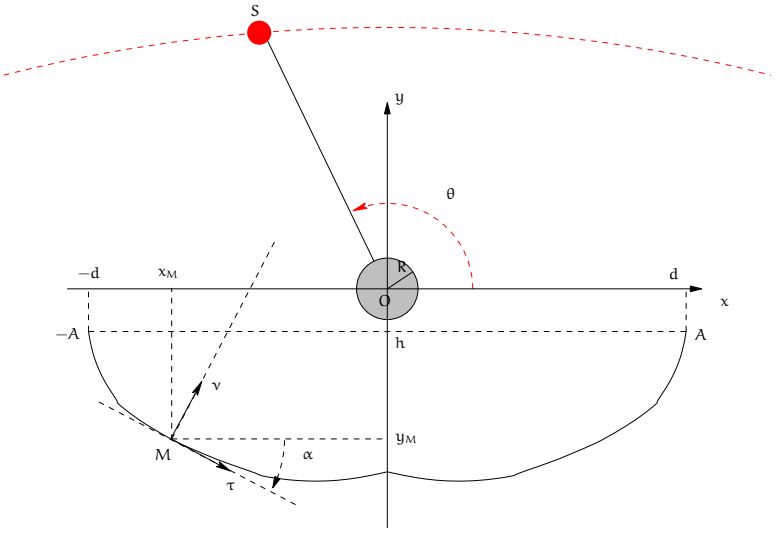

Figure 7: Problem statement.

A point M of the mirror will be illuminated by the for angles of Sun verifying

$$\theta \in (\beta_-, \beta_+) \setminus (\gamma_-, \gamma_+). \tag{5.2}$$

where all angles are defined on Figure 8. This corresponds to the red area. The four angles may be expressed as function of the point position and other geometry parameters:

$$\begin{aligned} \beta_\pm &= \arccos\left(\frac{\pm d - x_M}{\sqrt{(\pm d - x_M)^2 + (h - y_M)^2}}\right), \\ \gamma_\pm &= \pi - \arccos\left(\frac{x_M}{\sqrt{x_M^2 + y_M^2}}\right) \pm \arctan\left(\frac{R}{\sqrt{x_M^2 + y_M^2}}\right). \end{aligned}$$

The absorber will collect energy from M when M is lit and the Sun rays are reflected on the absorber. A necessary condition for the Sun rays to be reflected on the absorber by M is that

$$\theta \in (\gamma'_-, \gamma'_+).$$

where

$$\gamma'_\pm = 2\alpha + \arccos\left(\frac{x_M}{\sqrt{x_M^2 + y_M^2}}\right) \pm \arctan\left(\frac{R}{\sqrt{x_M^2 + y_M^2}}\right).$$

This is illustrated by Figure 9. Combining this result with (5.2), the absorber will collect solar energy from M exactly for

$$\theta \in I_M := \Big((\beta_-, \beta_+) \setminus (\gamma_-, \gamma_+)\Big) \cap (\gamma'_-, \gamma'_+).$$

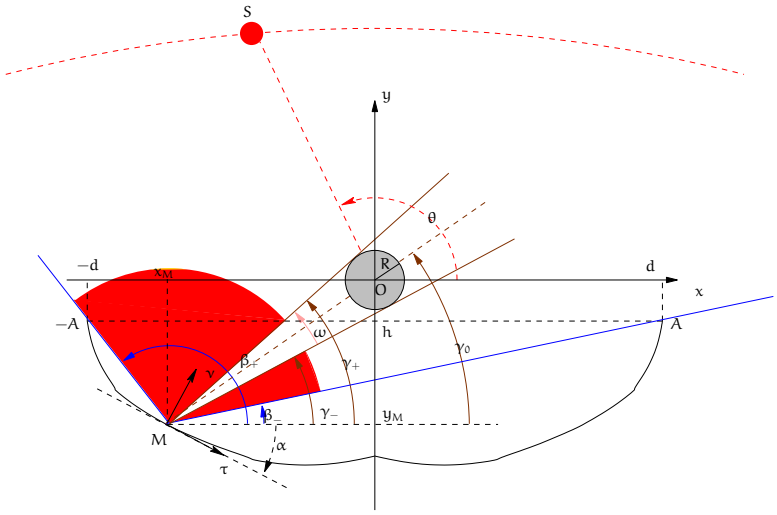

Figure 8: Enlightenment of M.

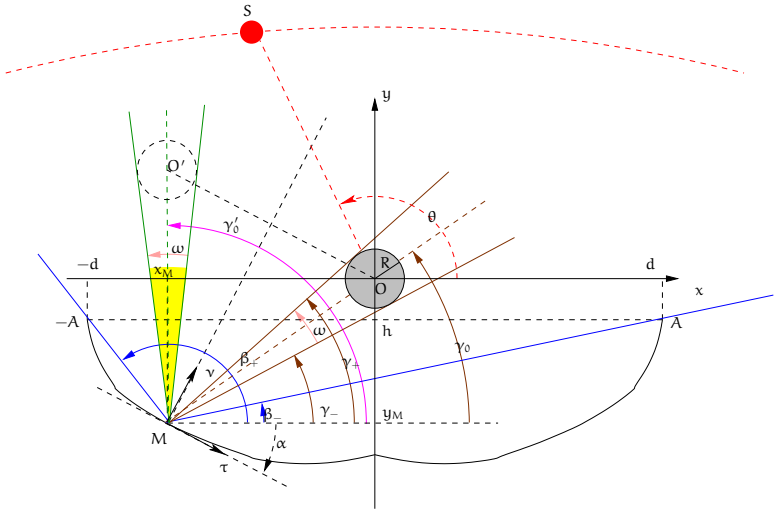

Figure 9: Image of the absorber by the reflector.

5.3 Optimisation algorithm

The mirror will now be determined using the following algorithm:

- The mirror is (numerically) divided into planar elements of width ds,
- The algorithm starts at the extremity of the aperture,
- Each element is positioned to maximise the energy reflected towards the collector.

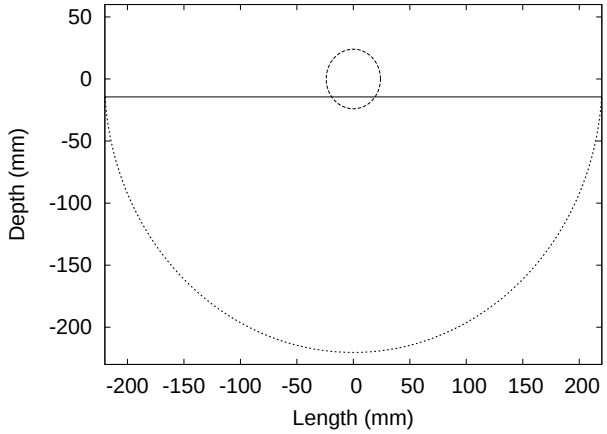

Figure 10: Mirror shape.

The energy reflected by an element of size ds inclined at an angle α to the horizontal as defined on Figure 9 is:

$$dE = P \int_{\theta \in I_M} \sin(\theta - \alpha) d\theta \ ,$$

where P is the energy radiated in the normal cross section of the solar beam. The value of dE should be maximised for each mirror element with respect to the inclination angle α. Note this parameter appears in the integral but also in the limits of the interval I_M.

Figure 10 shows the position of the collector and the shape of the mirror for a collector radius $R = 24$mm and an aperture of 440mm. As could be expected, most of the collector is located outside the mirror and this guarantees maximum direct energy hits for most of the day. The mirror shape resembles a parabola but its width differs by up to 20%. The shape is about 200mm deep. This is far from ideal from a building perspective but the model only includes first reflections. The shape of the mirrors should be significantly modified when further reflections are considered, particularly at the vertical of the collector and this would certainly reduce the depth of the mirror. The shape is also dependent on the optimisation method. Another optimisation method could lead to a different mirror shape. Further investigations are required to complete the study.

6 Optimisation

In this final section, the mirror shape is optimised for a device with a circular absorber located in Limerick, at latitude 50°N40'. The concentrator is assumed to be horizontal, aligned east-west and polar mounted, i.e. tilted south by the latitude angle. For each shape, the annual energy collected by the device is calculated using the theory in Section 2 and the ray tracing algorithm in Section 3, which determines the transmission function, $\mathcal{T}(\xi)$. Optimisation of

the mirror shape was performed using a swarm optimisation algorithm [15] coupled with basic Monte Carlo methods, and the depth of the device was constrained to be less than or equal to the typical depth of a frame installation. The algorithm was initialised with a given shape of the mirror, such as a parabola, involute or any other adequate geometry, and specified by a specific number of points. The optimisation process is extremely time consuming as the annual energy collected must be recalculated for every change in the shape, which involves recomputing the transmission function using the ray tracing algorithm at every step. Hence in practice, the mirror shape was only defined by 20 points. The results presented in this section are calculated for the standard element width of 440mm. The figures are scaled with the collector radius; 1 unit on the figure corresponds to 24mm. The designs are evaluated using the four following parameters:

- OOD is the Output Of Driver2_line is the ratio the energy collected and the actual energy available in the aperture.
- EPA is the Energy Per Absorber. This may be expressed as the OOD multiplied by the size of a frame and divided by the numbers of absorbers.
- TE stands for Total Energy. This is the product of the EPA and the number of absorbers. In the present study, the total size of the frame is 10.
- EPC describes the total Energy Per unit Cost. This is the parameter to be maximised and may be expressed as the Total Energy TE divided by the cost of the unit frame and absorbers (40 euros for the frame and 20 euros for the absorber)

6.1 Example 1

In this first example, the half aperture corresponds to 10 times the radius of the collector. There is one collector for each standard 440mm frame. The shape of the mirror may be seen in Figure 11.

The coordinates of the points are

x coordinate	-10	-8.9	-7.8	-6.7	-5.5
y coordinate	2.6557	3.2461	1.0585	-0.7331	-2.0026
x coordinate	-4.4	-3.3	-2.2	-1.1	0
y coordinate	-1.0434	-2.0939	-1.8143	-2.1132	-2.0893

This geometry leads to the following results

OOD	EPA	TE	EPC
0.2955	2.955	2.955	4.925

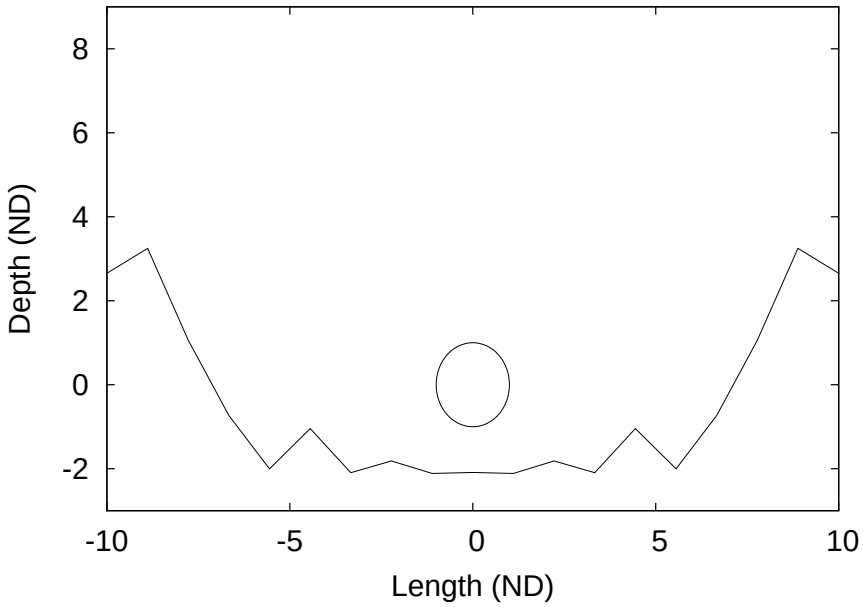

Figure 11: Collector 1.

6.2 Example 2

The half aperture corresponds now to 5 times the radius of the collector. There are two collectors for each standard 440mm frame. The shape of the mirror may be seen in Figure 12.

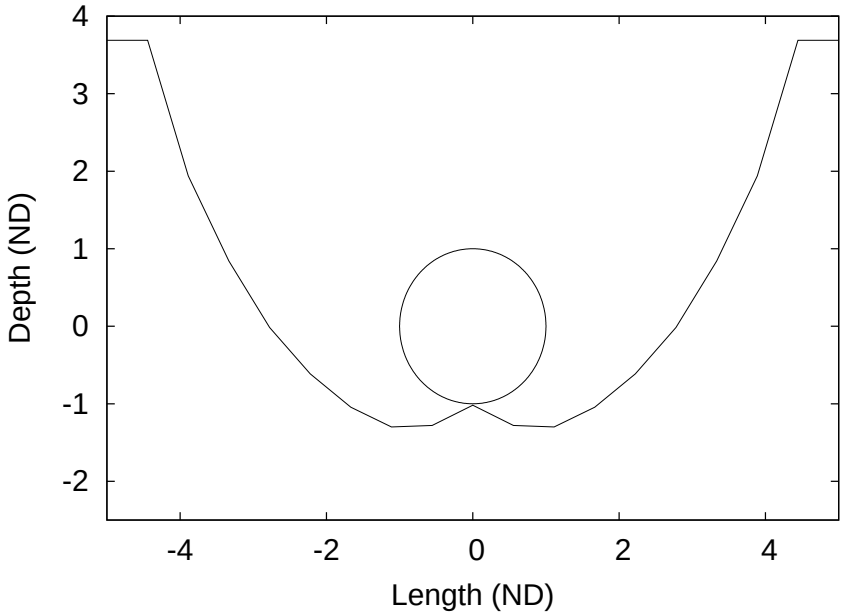

Figure 12: Collector 2.

The coordinates of the points are

x coordinate	-5	-4.4	-3.9	-3.3	-2.8
y coordinate	3.6882	3.6881	1.9397	0.8423	-0.0158
x coordinate	-2.2	-1.7	-1.1	-0.6	0
y coordinate	-0.6145	-1.0438	-1.2990	-1.2802	-1.0180

This geometry leads to the following results

OOD	EPA	TE	EPC
0.5974	2.987	5.974	7.4675

6.3 Example 3

In this example, the half aperture corresponds to 3.3 times the radius of the collector. There are three collectors for each standard 440mm frame. The shape of the mirror may be seen in Figure 13.

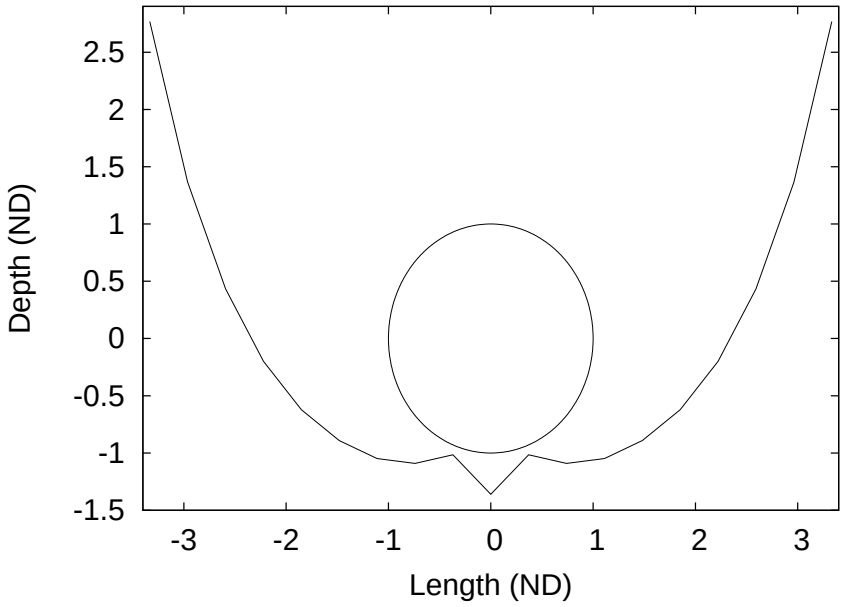

Figure 13: Collector 3.

The coordinates of the points are

x coordinate	-3.3	-3	-2.6	-2.2	-1.9
y coordinate	2.7680	1.3661	0.4321	-0.1994	-0.6211
x coordinate	-1.5	-1.1	-0.7	-0.4	0
y coordinate	-0.8910	-1.0479	-1.0910	-1.0156	-1.3600

This geometry leads to the following results

OOD	EPA	TE	EPC
0.7189	2.396	7.189	7.189

6.4 Example 4

In this final example, the half aperture corresponds to 2.5 times the radius of the collector. There are four collectors for each standard 440mm frame. The shape of the mirror may be seen in Figure 14.

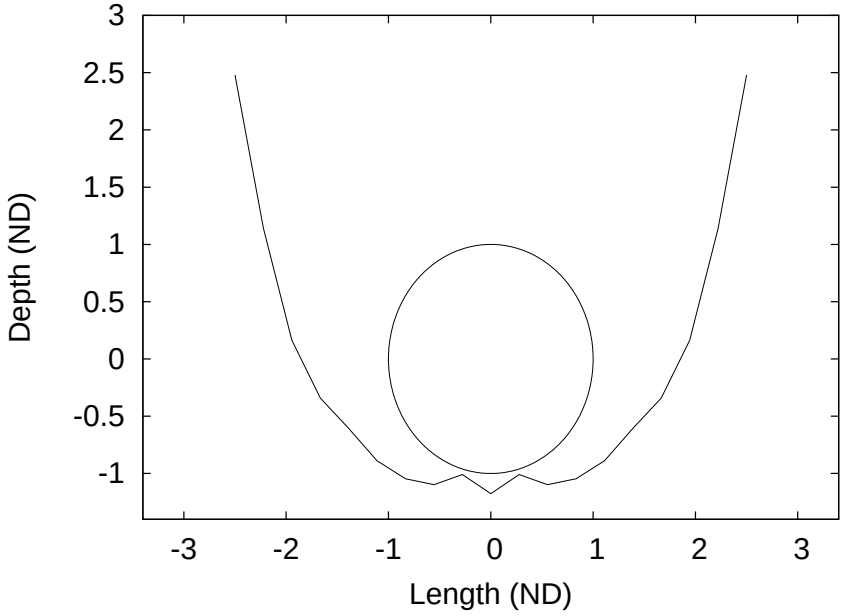

Figure 14: Collector 4.

The coordinates of the points are

x coordinate	-2.5	-2.2	-1.9	-1.6	-1.4
y coordinate	2.4792	1.1390	0.1641	-0.3419	-0.6071
x coordinate	-1.1	-0.8	-0.55	-0.3	0
y coordinate	-0.8888	-1.0460	-1.0977	-1.0092	-1.1762

This geometry leads to the following results

OOD	EPA	TE	EPC
0.7361	1.840	7.361	6.314

The EPC is maximum for two or three collectors per standard frame. The length of the aperture should therefore be reduced to maximise the cost efficiency of the device when a shallow depth is imposed.

7 Conclusion and future work

This reports details several aspects of the modelling problem submitted by Erin Energy. The solar radiation was studied and a ray tracing algorithm was developed. Several techniques were then presented to calculate the shape of the device. The optimisation process shows that wide (and shallow) reflectors are not as energy efficient as smaller devices: for the standard 440mm length, two to three devices should be more economically efficient than a single optimised device when the depth of the mirror is forced to remain shallow.

Future work could be done in the following directions:

- The optimisation should be performed much more systematically. The present study limited the research to 20 points in the last section, many more should be used.
- The optimisation process was initialised using a limited number of shapes. More should be considered, such as the shapes calculated using the inverse method or the one reflection approach.
- Finally the optimisation should be performed for other orientations of the concentrator, e.g. with north-south alignment, and inclined by the angle of pitch of a typical roof.

Acknowledgements

The contributions of Giles Richardson and Galin Ganchev are here kindly acknowledged. All contributors would like to thank Mr Sean Hoolan from Erin Energy Ltd for introducing the problem and assisting in answering questions during the entire week. J.P.F. Charpin, R. Gaburro

and S. Soussi acknowledge the support of the Mathematics Applications Consortium for Science and Industry (www.macsi.ul.ie) funded by the Science Foundation Ireland mathematics initiative grant 06/MI/005.

Bibliography

[1] J.A. Duffie and W.A. Beckman. *Solar Engineering of Thermal Processes*. John Wiley and Sons Inc, third edition, 2006.

[2] W.B. Stine and R.W. Harrigan. *Solar Energy Systems Design*. John Wiley and Sons Inc, 1985.

[3] C.G. Bell, M. McCulloch, H. Ockendon and J.R. Ockendon. Annual energy distribution on stationary solar collectors. To be submitted.

[4] H.C. Hottel. A simple model for estimating the transmittance of direct solar radiation through clear atmospheres. *Sol. Energy*, 18(2):129-134, 1976.

[5] A. Rabl. Comparison of solar collectors. *Sol. Energy*, 18(2):93-111, 1976.

[6] J.J. Duistermaat. *Fourier Integral Operators*. Birkhauser, Boston, 1996.

[7] A. Grigis and J. Sjöstrand. *Microlocal Analysis for Differential Operators: an Introduction*, volume 196 of *London Mathematical Society Lecture Note Series*. Cambridge University Press, 1994.

[8] F. Treves. *Introduction to Pseudodifferential and Fourier Integral Operators*, volume I and II. Plenum Press, New York, 1980.

[9] M. Cheney. A mathematical tutorial on synthetic aperture radar. *SIAM Rev.*, 43:301-312, MR:1861084, 2001.

[10] R. Gaburro and C. J. Nolan. Enhanced imaging from multiply scattered waves. *Inverse Probl. Imag.*, 2:1-20, 2008.

[11] R. Gaburro, C. J. Nolan, T. Dowling and M. Cheney. Imaging from multiply scattered waves. SPIE 6513, 2007. Article 651304.

[12] C. J. Nolan and M. Cheney. Synthetic aperture inversion for arbitrary flight paths and non-flat topography. *IEEE T. Image Process.*, 12:1035-1043, MR:2006858, 2003.

[13] C. J. Nolan and M. Cheney. Synthetic aperture inversion. *Inverse Probl.*, 18:221-236, 2002.

[14] C. J. Nolan, M. Cheney, T. Dowling and R. Gaburro. Enhanced angular resolution from multiply scattered waves. *Inverse Probl.*, 22:1817-1834, MR:2261268, 2006.

[15] A.I.F. Vaz and L.N.Vicente. A particle swarm pattern search method for bound constrained global optimization. *J. Global Optim.*, 39:197-219, 2007.